TECHNIQUE

An Accurate, Robust, and Computationally Efficient Navigator Algorithm for Measuring Diaphragm Positions[#,‡]

Yiping P. Du, Ph.D.,[1,*] Manojkumar Saranathan, Ph.D.,[2] and Thomas K. F. Foo, Ph.D.[2]

[1]Departments of Psychiatry and Radiology, University of Colorado Health
Sciences Center, Denver, Colorado, USA
[2]Applied Science Laboratory, GE-Medical Systems, Milwaukee, Wisconsin, USA

ABSTRACT

Purpose: The purpose of this study is to develop an improved algorithm for measuring the position of the diaphragm using navigator echoes. *Method:* This algorithm was applied to navigator echo data acquired from 14 cardiac patients. For each patient, 160 navigator echo profiles were acquired across the right hemi-diaphragm along the superior-inferior direction. *Results:* The accuracy of the proposed edge-detection algorithm was evaluated together with that of the least-squares and linear phase-shift algorithms. The estimated measurement error of the proposed algorithm was approximately two times smaller than that of the least-squares algorithm (Magn Reson Med, 1996:36: 117–123), and was approximately four times smaller than that of the linear phase-shift algorithm (Magn Reson Med, 1999;42:548–553). The computational efficiency of this algorithm was 7.5 times higher than that of the least-squares algorithm and was comparable with that of the linear phase-shift algorithm. *Conclusion:* The presented algorithm is accurate, robust, and computationally efficient in the measurement of the diaphragm position.

Key Words: MR imaging; Navigator echo; Coronary artery imaging; Respiratory compensation.

INTRODUCTION

Three-dimensional (3D) magnetic resonance coronary angiography (MRCA) has the advantages of being able to obtain thinner partitions, having higher image signal-to-noise ratio (SNR), and the ability to reformat the resulting volume in any arbitrary plane (Hofman et al., 1995; Li et al., 1993). However, 3D MRCA is prone to respiratory motion artifacts because of the prolonged imaging time. To avoid these artifacts one can use navigator echo gating techniques (Ehman and Felmlee, 1989; Korin et al., 1990), which rely on an accurate and effective algorithm to determine the diaphragm position prior to data acquisition. This allows free-breathing 3D MRCA examinations with superior image quality (Li et al., 1996; Liu et al., 1993; Wang et al., 1995a,1996a).

Accurate detection of respiratory motion is essential for proper respiratory gating (Jhooti et al., 1998; Sachs et al., 1994, 1995) and adaptive motion correction (Danias et al., 1997). A successful navigator algorithm for clinical applications of MRCA has to be accurate, robust, and computationally efficient. Cross-correlation (Wang et al., 1996b), least-squares (Wang et al., 1996b), and linear phase-shift (Foo and King, 1999) techniques have all been used to determine the diaphragm position from a projection image across the right hemi-diaphragm. These algorithms use the shift of signal intensity profile of a navigator echo to characterize the motion of the diaphragm. The deformation of the liver and the lung during breathing introduces variation in the intensity profile and error in these algorithms. Wang et al. (1996b) and our experiments have shown that significant errors occur when the cross-correlation algorithm was used. The least-squares algorithm provides improved measurement accuracy compared with the cross-correlation algorithm and the linear phase-shift algorithm. The computational efficiency of the least-squares algorithm, however, is similar to that of the cross-correlation algorithm and is substantially lower than that of the linear phase-shift algorithm (Foo and King, 1999). More recently, a k-space weighted least-squares algorithm was also proposed to improve the robustness against noise (Nguyen et al., 2001).

The position of the diaphragm can be detected directly from the intensity profile. The lung, which has a very low SNR, and the diaphragm/liver form a well-defined edge in the signal intensity profile of a navigator echo. An algorithm that uses an averaging (smoothing) filter and a high-pass filter to extract the edge of the diaphragm in a navigator profile was initially proposed by Liu et al. (1993). Unfortunately, this approach is sensitive to image noise and has low

accuracy in locating the edge. Another thresholding algorithm has been proposed to detect the edge of the diaphragm for navigated 3D MRCA (Hofman et al., 1995; Li et al., 1996); however, the detail of the algorithm and the evaluation of performance and computational efficiency were not reported in these studies. In this paper, we present a new edge-detection navigator algorithm for fast, accurate, and robust measurement of diaphragm displacement. We evaluate the accuracy and computational efficiency of this algorithm in comparison with other commonly used algorithms. This algorithm can be applied to navigated 3D MRCA.

METHODS

Data Acquisition

Navigator echo data across the right hemi-diaphragm were acquired in 14 cardiac patients, eight men and six women, with ages ranging from 26 to 56 years. Informed, written consent was obtained from all the subjects prior to the scan. Experiments were performed on 1.5 T CV/iMR scanners (GE Medical Systems, Waukesha, WI). For each patient, 160 navigator echo data projections were acquired in consecutive heartbeats during free breathing with an echocardiogram (ECG)-gated, navigated 3D gradient-echo pulse sequence using a four-element phased-array coil. The total data acquisition time was 160 heartbeats. In the navigator portion of this pulse sequence, a selective 90° pulse was used to excite a 20-mm slab along the sagittal direction, and a selective 180° pulse was applied to a 20-mm oblique sagittal slab that was rotated 45° along the superior/inferior axis to avoid saturating the heart. The navigator echo signal from the intersection of these two planes was detected. The field-of-view (FOV) of the one-dimensional (1D) navigator profile was 100 mm. The readout bandwidth was ±16 kHz, and 128 complex data points were acquired for each of the navigator echoes. The k-space data of the navigator echo acquisition were saved in a file for postprocessing. The overall duration of the navigator was 32 ms, including 10 ms for data acquisition.

Algorithm

The implementation of this algorithm includes the following steps:

1. Obtain a navigator profile, g(x), after the Fourier transform of the navigator echo, where x is the positional index.
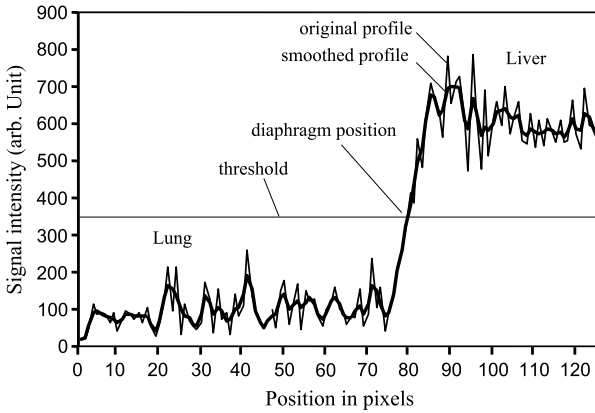
Figure 1. A navigator profile with low SNR. The threshold is set at the middle of the maximum intensity of the smoothed profile. The crossing point of the profile and the threshold is defined as the position of the diaphragm edge.

2. Smooth the navigator profile by convolving the navigator profile with a triangular smoothing function. The smoothed navigator profile $f(x)=0.25*g(x-1)+0.5*g(x)+0.25*g(x+1)$. The smoothing of the profile improves the performance of the algorithm, especially when the SNR of the profile is low (Fig. 1). A triangular smoothing function was selected because of its high computational efficiency.

3. Set a threshold value, f_{th}, at the half-value of the maximum intensity for each of the smoothed profiles. Because the orientation of the diaphragm surface may not be perpendicular to the navigator excitation, the edge of the diaphragm may not always be sharp in the navigator profile. The ''edge'' of the diaphragm in the navigator profile is defined to be the location where the navigator profile intersects with the threshold value. Although other approaches can be used to determine the threshold value and the location of ''edge'' in the navigator profile, we used the half-value of the maximum intensity in the smoothed navigator profile for simplicity.

4. Apply an edge-detection operation from the low signal end (i.e., lung) to the high signal end (i.e., liver) of the navigator profile. This edge-detection operation compares the intensities of the current point, $f(x)$, and the next point, $f(x+1)$, to the threshold value, f_{th}. A rising edge is detected when the following condition is met:

$$f(x) < f_{th} < f(x+1) \qquad (1)$$

When an edge is detected, the position of the edge, P_{edge}, is calculated using a linear interpolation: $P_{edge}=x+(f_{th}-f(x))/(f(x+1)-f(x))$, where P_{edge} is the position of the detected edge in the unit of the pixel size of the navigator profile. In prospective gating, this edge-detection operation only needs to be conducted within the gating window.

5. If an edge is detected, the edge-detection operation is applied to the next N_w points. If a falling edge is detected at point j ($j<P_{edge}+N_w$):

$$f(j) > f_{th} > f(j+1) \qquad (2)$$

the detected edge value is discarded. In navigator data with low image SNR, a noise spike, or a large vessel in the lung, can be erroneously identified as a diaphragm edge. These false detections of the edge can be identified and discarded by this condition. In this situation, no valid edge is found by the algorithm. The selection of N_w should be such that 1) the signal variation due to noise spikes or local structures, such as vessels in the lung, does not generate false detection of the edge; 2) the signal drop at the inferior portion of the liver due to the sensitivity fall-off of the surface coil does not affect the edge detection. In this experiment, we selected $N_w = 8$, or a width of 6.25 mm in the navigator profile.

Measurement of Accuracy

Previously, the position of diaphragm was measured at its midpoint on a set of 2D ECG-gated coronal images acquired at different levels of breath-hold (Wang et al., 1995b). This method is not feasible for measuring the position of diaphragm during free breathing, because the data acquisition time for a 2D image is on the order of 18 heart beats. Measurement errors can therefore occur even in multiple breath-holds because 1) the placement of the measurement markers cannot be more precise than the size of displayed pixels; 2) human error in the placement of the markers. Here, we address the source of these errors by: 1) Measuring the position of diaphragm using the 1D navigator instead of a 2D image to reduce data acquisition time. In our study, a 1D navigator was acquired in a time period less than 10 ms; the respiratory motion is negligible in such a short duration; 2) Zero-filling the navigator echoes in the k-space from 128 to 512 points in order to obtain a more faithful representation of the true intensity profile of the
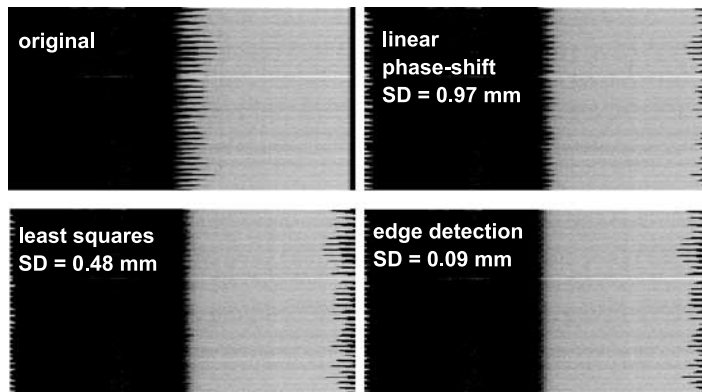
Figure 2. Navigator profiles aligned using the measurements from the linear phase-shift, least-squares, and edge-detection algorithms. The figures on the right side are the enlarged view of the figures on the left side for better visualization of the edge alignment.

diaphragm; and 3) Avoiding human error by using a threshold to estimate the measurement error.

Before the measurement, the edge position of a selected navigator profile (e.g., the first navigator profile) was selected as the reference position. Each of the algorithms was applied to the navigator echo data to measure the displacement of the diaphragm relative to the reference position during free breathing. A linear phase-shift term was applied to the complex navigator echo so that the navigator profile obtained after the Fourier transform was circularly shifted relative to the reference position by the same amount, but in the opposite direction, to that of the diaphragm displace-

ment. This approach can shift the profile by any amount without introducing errors that are associated with interpolating the sampling points in the spatial domain. It also provides a visual examination of the accuracy of the measurement: after shifting the navigator profile towards the reference position, an accurate measurement of the displacement will result in a "straight" line-up of the profiles; an inaccurate measurement of diaphragm displacement results in a "jagged" line-up of the profiles. The alignment of 160 navigator profiles for one patient scan is shown in Fig. 2.

To quantitatively assess the accuracy of each algorithm, a single threshold was set at half the maximum
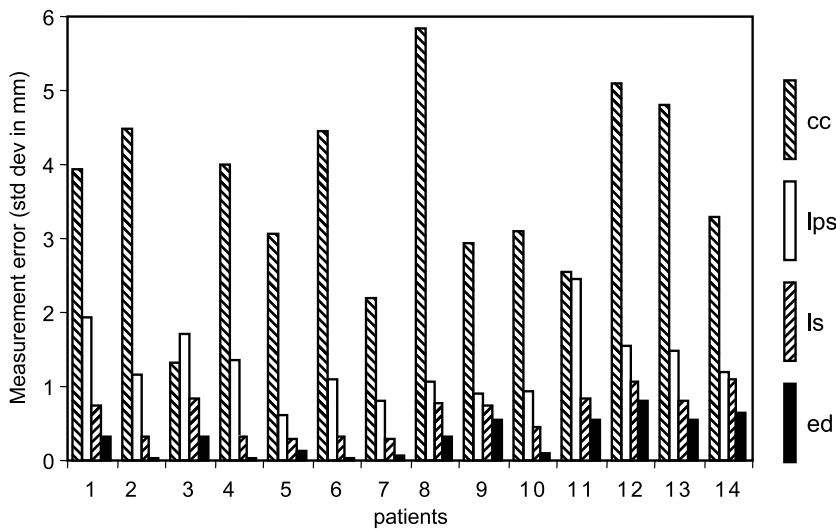
Figure 3. Standard deviation of measurement error in mm using the cross-correction (cc), linear phase-shift (lps), least-squares (ls), and edge-detection (ed) algorithms. The edge-detection algorithm has the smallest measurement error in all the 14 patient studies.

intensity of each of the zero-filled and aligned navigator profiles. The intersection of this threshold and the navigator profile was considered to be the position of diaphragm. The mean edge position of the aligned navigator profiles can then be calculated. The measurement error was estimated by the standard deviation of the edge positions of the 160 aligned navigator profiles from their mean.

RESULTS

The cross-correlation, least-squares, and linear phase-shift algorithms were all applied to the same navigator data sets as well as the proposed edge-detection algorithm. A comparison of the measurement accuracy between these algorithms and the edge-detection algorithm was performed.

The original navigator profiles from a typical patient study are shown in Fig. 2. The same navigator profiles aligned with the measurements obtained by applying the linear phase-shift, least-squares, and edge-detection algorithms are also shown in Fig. 2.

The edge of the diaphragm was successfully found in each of the 160 navigator echoes for 10 of the 14 patient scans. In the other four patient scans with low SNR, a valid edge was found in more than 97% of the navigator profiles. All edges detected by the algorithm were identified visually to be the true edges of the diaphragm in all the scans.

The measurement error of each algorithm for the 14 patient studies is shown in Fig. 3. The overall mean and standard deviation of the measurement error can be found in Table 1. The results show that the estimated measurement error with the edge-detection algorithm was approximately two times smaller than that of the least-squares algorithm and about four times smaller than that of the linear phase-shift algorithm [analysis of variance (ANOVA), $F = 66$, $p < 0.001$].

*Table 1.* Computational efficiency and overall measurement error of the navigator algorithms.

Algorithms	Computational efficiency (number of operations for N=128)	Mean (SD) (mm)
Cross-correlation	46336	3.65 (1.22)
Linear phase-shift	8192	1.31 (0.48)
Least squares	54528	0.66 (0.28)
Edge detection	7296	0.33 (0.28)

DISCUSSION

A major challenge of the edge-detection algorithm is the fact that the navigator profiles can sometimes have low SNR. For example, in large patients, the navigator signal is reduced because of the fall-off of the coil sensitivity at a greater depth. The navigator signal can also suffer when the receiver coil or the navigator excitation column is not properly placed. To minimize artifacts, it is crucial that the edge-detection algorithm performs properly even in low SNR situations.

When the SNR of the navigator profile is poor, smoothing of navigator profiles improves the robustness of the edge-detection algorithm by reducing noise spikes. The smoothing operation was implemented by convolving the original profile with a smoothing function, that can be a rectangular window function, or a bell-shaped function. The effectiveness of removing noise spikes and the degree of blurring are determined by the full-width at half maximum of the smoothing function. The computational complexity of the smoothing operation is determined by the full width of the smoothing function. In this study, we found that a normalized three-point triangle function (0.25, 0.5, 0.25) effectively smoothes the profile without introducing significant computational complexity, although other smoothing functions may also be used. The navigator smoothing operation can possibly compromise the resolution of the edge detection. Because the smoothing operation was performed to the interpolated navigator profile, we expect that the ''blurring'' caused by the smoothing operation was smaller than the size of the interpolated pixel. The benefit of reducing false edge detection outweighs the compromise in the resolution of edge detection, especially when the SNR is low. The error introduced by the smoothing operation in the measurement of relative displacement of the diaphragm is expected to be much smaller than the blurring, because all the navigator profiles experience the same degree of blurring after the smoothing operation.

False edge detection can occur even after smoothing the navigator profile. To remove erroneously detected edge, the algorithm searches N_w points forward after a rising edge is detected to ensure that no falling edge occurs in the neighborhood of the rising edge. If a falling edge is found, the detected rising edge is considered as a false edge and no valid edge is assigned to this navigator profile. In this study, the robustness of this edge detection is manifested by the following observation: a valid edge was found in more that 97% of the navigator profiles even in studies with low SNR; visual examination indicated that the edge
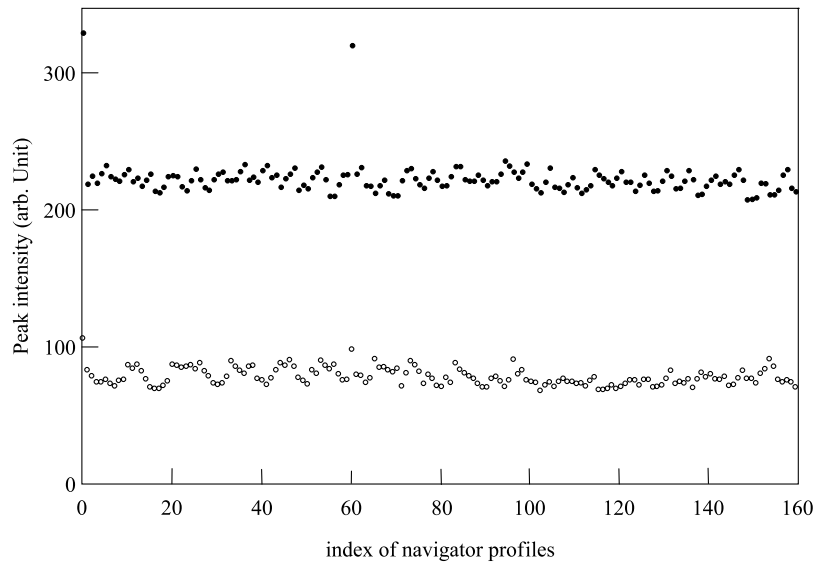
Figure 4. The variation of peak profile intensity from a study with high SNR (top plot) and from a study with low SNR (bottom plot). The peak intensity is higher at the first navigator profile because the magnetization has not been saturated; and at the 61st navigator profile due to a pause of 2−3 seconds in the sequence. The variation of the peak profile intensity reflects the variation of effective repetition time (TR) during data acquisition.

detected was the true edge in each of the navigator profiles for all 14 patient studies.

The intensity of the navigator profile varies from one heart beat to another. Large signal variations can occur due to variable T1 relaxation when a patient has severe arrhythmias. The maximum intensities of 160 navigator profiles acquired from a patient study are shown in Fig. 4. The first navigator profile has a higher intensity because the data were acquired before the magnetization reached steady-state. The 61st profile also has a higher intensity because the pulse sequence has a pause of 2−3 seconds after acquiring 60 reference navigator echoes in order to calculate the most repeatable position as the reference position. The variation of maximum intensity observed in other navigator profiles was largely due to the variation in heart rate. A theoretical estimation shows that a change in heart rate from 80 to 70 beats/min can increase the signal of liver (T1 = 500 ms) by 6%, comparable to the signal variation in the top plot in Fig. 4. The variation of signal intensity of the navigator profiles was addressed by setting a threshold relative to its maximum value.

The cross-correlation, least-squares, and linear phase-shift algorithms assume that the breathing introduces a ''rigid body'' motion of the lung and the liver. However, in our experiments we observed considerable expansion and compression of the lung and the liver along the superior/inferior (S/I) direction during breathing. We believe that this discrepancy between a ''rigid body'' model and the elastic nature of the lung and liver is the major cause of errors in these algorithms. To the contrary, the edge detection algorithm does not assume a ''rigid body'' motion of the lung and the liver.

Computational Efficiency of a navigator algorithm is an important factor for prospective gating. A 1D Fourier transform has approximately $6 N\log_2 N$ operations for a navigator echo with N complex data points. Computing the magnitude, smoothing the profile, and detecting the edge take approximately $13 N$ operations (i.e., magnitude: $4 N$; smoothing: $3 N$; detecting edge: $6 N$). The total number of operations of the edge-detection algorithm is approximately $6 N\log_2 N + 13 N$ for each navigator echo. The results of similar analysis for each of the algorithms are listed in Table 1. Note that the computational efficiency of the edge-detection algorithm is much higher than that of either the cross-correlation and the least-squares algorithm, and is slightly higher than that of the linear phase-shift algorithm. Using any of these navigator algorithms in prospective gating, the search for the edge only needs to be conducted within the gating window. Therefore, the computation efficiency is inversely proportional to the width of the gating window. In the current implementation (Du, 2003), the overall duration of the navigator was 32 ms, including 10 ms for data acquisition and 22 ms for transferring the data to a

separate processing engine, calculating the diaphragm displacement with the navigator algorithm, and transferring back the calculated results. Within the 22 ms, the time for data transferring is much longer than the time for navigator calculation. As a result, the actual time benefit of the edge detection algorithm was less than 1 ms. This time benefit can become more significant when the speed of data transferring is improved and when a higher resolution navigator (e.g., 256 sampling points) is used. In this experiment, we interpolated the navigator echoes using the zero-filled interpolation algorithm prior to edge detection to obtain subpixel accuracy. Although this approach is simple in implementation, other interpolation schemes may also be used. For example, sinc interpolation performed in a small region nearby the edge can achieve the same subpixel accuracy with an improved computational efficiency.

CONCLUSION

The edge-detection algorithm provides more accurate measurement of diaphragm displacement compared to the least squares and other navigator algorithms. This algorithm has robust performance at low SNR and high signal variation caused by arrhythmia. The high accuracy and robustness of this algorithm as well as its computational efficiency make it an excellent candidate for prospective respiratory gating and adaptive motion correction on an MR scanner.

ACKNOWLEDGMENTS

REFERENCES

Danias, P. G., McConnell, M. V., Khasgiwala, V. C., Chung, M. L., Edelman, R. R., Manning, W. J. (1997). Prospective navigator correction of image position for coronary MR angiography. *Radiology* 203:733–736.

Du, Y. P. (2003). Prospective navigator gating with a dual acceptance window technique to reduce respiratory motion artifacts in 3D MR coronary angiography. *Int. J. Card. Imaging* 19:157–162.

Ehman, R. L., Felmlee, J. P. (1989). Adaptive technique for high-definition MR imaging of moving structures. *Radiology* 173:255–263.

Foo, T. K. F., King, K. F. (1999). A computationally efficient method for tracking reference position displacement for motion compensation in magnetic resonance imaging. *Magn. Reson. Med.* 42:548–553.

Hofman, M. B. M., Paschal, C. B., Li, D., Haacke, E. M., van Rossum, A. C., Sprenger, M. (1995). MRI of coronary arteries: 2D breath-hold vs 3D respiratory-gated acquisition. *J. Comput. Assist. Tomogr.* 19:56–62.

Jhooti, P., Wiesmann, F., Taylor, A. M., Gatehouse, P. D., Yang, G. Z., Keegan, J., Pennell, D. J., Firmin, D. N. (1998). Hybrid ordered phase encoding (HOPE): an improved approach for respiratory artifact reduction. *J. Magn. Reson. Imaging* 8:968–980.

Korin, H. W., Felmlee, J. P., Ehman, R. L., Riederer, S. J. (1990). Adaptive technique for three dimensional MR imaging of moving structures. *Radiology* 177:217–221.

Li, D., Paschal, C. B., Haacke, E. M., Adler, L. P. (1993). Coronary arteries: three-dimensional MR imaging with fat saturation and magnetization transfer contrast. *Radiology* 187:401–406.

Li, D., Kaushikkar, S., Haacke, E. M., Woodard, P. K., Dhawale, P. J., Kroeker, R. M., Laub, G., Kuginuki, Y., Gutierrez, F. R. (1996). Coronary arteries: three-dimensional MR imaging with retrospective respiratory gating. *Radiology* 201:857–863.

Liu, Y. L., Riederer, S. J., Rossman, P. J., Grimm, R. C., Debbins, J. P., Ehman, R. L. (1993). A monitoring, feedback, and triggering system for reproducible breath-hold MR imaging. *Magn. Reson. Med.* 30:507–511.

Nguyen, T. D., Wang, Y., Watts, R., Mitchell, I. (2001). K-space weighted least-squares algorithm for accurate and fast motion extraction from magnetic resonance navigator echoes. *Magn. Reson. Med.* 46:1037–1040.

Sachs, T. S., Meyer, C. H., Hu, B. S., Kohli, J., Nishimura, D. G., Macovski, A. (1994). Real-time motion detection in spiral MRI using navigators. *Magn. Reson. Med.* 32:639–645.

Sachs, T. S., Meyer, C. H., Irarrazabal, P., Hu, B. S., Nishimura, D. G., Macovski, A. (1995). The diminishing variance algorithm for real-time reduction of motion artifacts in MRI. *Magn. Reson. Med.* 34:412–422.

Wang, Y., Grimm, R. C., Rossman, P. J., Debbins, J. P.,

Riederer, S. J., Ehman, R. L. (1995a). 3D coronary MR angiography in multiple breath-holds using a respiratory feedback monitor. *Magn. Reson. Med.* 34:11–16.

Wang, Y., Riederer, S. J., Ehman, R. L. (1995b). Respiratory motion of the heart: kinematics and the implications for the spatial resolution in coronary imaging. *Magn. Reson. Med.* 33:713–719.

Wang, Y., Rossman, P. J., Grimm, R. C., Riederer, S. J., Ehman, R. L. (1996a). Navigator-echo-based real-time respiratory gating and triggering for reduction of respiratory effects in three-dimensional coronary MR angiography. *Radiology* 198: 55–60.

Wang, Y., Grimm, R. C., Felmlee, J. P., Riederer, S. J., Ehman, R. L. (1996b). Algorithms for extracting motion information from navigator echoes. *Magn. Reson. Med.* 36:117–123.

Request Permission or Order Reprints Instantly!